

This document contains a post-print version of the paper

Efficient numerical computation of direct exchange areas in thermal radiation analysis

authored by M. Feischl, T. Führer, M. Niederer, S. Strommer, A. Steinboeck, and D. Praetorius
and published in *Numerical Heat Transfer, Part B: Fundamentals*.

The content of this post-print version is identical to the published paper but without the publisher's final layout or copy editing. Please, scroll down for the article.

Cite this article as:

M. Feischl, T. Führer, M. Niederer, S. Strommer, A. Steinboeck, and D. Praetorius, "Efficient numerical computation of direct exchange areas in thermal radiation analysis", *Numerical heat transfer, part b: Fundamentals*, vol. 69, no. 6, pp. 511–533, 2016. DOI: [10.1080/10407790.2016.1173469](https://doi.org/10.1080/10407790.2016.1173469)

BibTex entry:

```
@ARTICLE{acinpaper,  
  AUTHOR = {Feischl, M. and Führer, T. and Niederer, M. and  
Strommer, S. and Steinboeck, A. and Praetorius, D.},  
  TITLE = {Efficient numerical computation of direct exchange  
areas in thermal radiation analysis},  
  JOURNAL = {Numerical Heat Transfer, Part B: Fundamentals},  
  YEAR = {2016},  
  volume = {69},  
  number = {6},  
  pages = {511--533},  
  doi = {10.1080/10407790.2016.1173469},  
  url = {http://www.tandfonline.com/doi/full/10.1080/10407790.2016.1173469}  
}
```

Link to original paper:

<http://dx.doi.org/10.1080/10407790.2016.1173469>
<http://www.tandfonline.com/doi/full/10.1080/10407790.2016.1173469>

Read more ACIN papers or get this document:

<http://www.acin.tuwien.ac.at/literature>

Contact:

Automation and Control Institute (ACIN)
Vienna University of Technology
Gusshausstrasse 27-29/E376
1040 Vienna, Austria

Internet: www.acin.tuwien.ac.at
E-mail: office@acin.tuwien.ac.at
Phone: +43 1 58801 37601
Fax: +43 1 58801 37699

Copyright notice:

This is the authors' version of a work that was accepted for publication in *Numerical Heat Transfer, Part B: Fundamentals*. Changes resulting from the publishing process, such as peer review, editing, corrections, structural formatting, and other quality control mechanisms may not be reflected in this document. Changes may have been made to this work since it was submitted for publication. A definitive version was subsequently published in M. Feischl, T. Führer, M. Niederer, S. Strommer, A. Steinboeck, and D. Praetorius, "Efficient numerical computation of direct exchange areas in thermal radiation analysis", *Numerical heat transfer, part b: Fundamentals*, vol. 69, no. 6, pp. 511–533, 2016. DOI: [10.1080/10407790.2016.1173469](https://doi.org/10.1080/10407790.2016.1173469)

Contributed Paper

EFFICIENT NUMERICAL COMPUTATION OF DIRECT
EXCHANGE AREAS IN THERMAL RADIATION ANALYSIS

Abbreviated title: EFFICIENT COMPUTATION OF DIRECT EXCHANGE AREAS

M. Feischl^a, T. Führer^a, M. Niederer^b, S. Strommer^b, A. Steinboeck^{b,*}, and D. Praetorius^a^a*Institute of Analysis and Scientific Computing, Vienna University of Technology,
Wiedner Hauptstraße 8, 1040 Vienna, Austria*^b*Automation and Control Institute, Vienna University of Technology,
Gußhausstraße 27–29, 1040 Vienna, Austria**(Received 7 September 2015; final version received 11 November 2015)*

Abstract: The analysis of thermal radiation in multi-surface enclosures typically involves multiple integrals with four, five, or six variables. Major difficulties for the numerical evaluation of these integrals are non-convex geometries and singular integral kernels. This paper presents hierarchical visibility concepts and coordinate transformations which eliminate these difficulties. In the transformed form, standard quadrature techniques are applied and accurate results are achieved with moderate numerical effort. In benchmark example problems, the effectiveness and accuracy of the method are validated. A simulation model of an industrial furnace demonstrates the applicability of the method for large-scale problems.

NOMENCLATURE

B_α	bounding box
b	radiosity, W/m ²
$C(\alpha)$	function for computing the visibility
D	integration domain
d	side length, distance, m
f	continuous function or part of the kernel k , m ⁴
g	part of the integral kernel k , 1/m ²
H	heat flux density absorbed by a volume zone, W/m ²

*Corresponding author. Email: andreas.steinboeck@tuwien.ac.at

h	irradiance, W/m^2
I	total intensity, $\text{W}/(\text{m}^2\text{sr})$
K	absorption coefficient, $1/\text{m}$
k	integral kernel, $1/\text{m}^4$
M	order of quadrature
N_S	number of surface zones
N_V	number of volume zones
\dot{Q}	net heat flow into volume zone, W
\dot{q}	net heat flow into surface zone, W
r	distance coordinate along a ray, m
r_j, r_{ij}	geometrical length of a ray, m
\bar{r}_{ij}	optical length of a ray
\mathcal{S}_α	set of barycenters of surfaces zones
$S(\alpha)$	functions for generating a hierarchy of bounding boxes
S	surface zone, surface area, m^2
s	evaluation point of Gaussian quadrature
$\overline{s_i s_j}$	surface-surface direct exchange area, m^2
$\overline{s_i v_j}$	surface-volume direct exchange area, m^2
T	gas temperature, K
t	surface temperature, K
V	volume zone, volume, m^3
V_{ref}	reference volume zone
$\overline{v_i s_j}$	volume-surface direct exchange area, m^2
$\overline{v_i v_j}$	volume-volume direct exchange area, m^2
W	integration domain
w	weight of Gaussian quadrature
\vec{x}	coordinates in volume zone, m
α	tuple
$\vec{\alpha}, \vec{\beta}$	normalized coordinates in reference volume zone
$\vec{\gamma}$	relative coordinates
ε	emissivity
θ	incident or emergent angle, rad
Λ	coordinate transformation
σ	Stefan-Boltzmann constant, $\text{W}/(\text{m}^2\text{K}^4)$
Φ	function for a transformation of integration domains

Subscripts

i, j index of zone or index value
 k, n index value

1. INTRODUCTION

Heat transfer by gray thermal radiation in enclosures formed by diffuse surfaces and filled with participating gas can be efficiently analyzed by means of the zone method [1]. Instead of a rigorous solution of the multiple integrals that emerge from the direct application of the radiative transfer equation [2, 3], the zone method uses a spatial discretization of the radiation geometry to obtain a finite-dimensional linear relation between the radiative heat flows and the fourth powers of the temperatures. The discretization is found by dividing the calculation domain into isothermal surface and volume sections. The approach may be considered as a numerical quadrature method that facilitates a direct geometric interpretation.

The zone method, which was originally suggested by Hottel and coworkers [1, 4], is described in detail in [2, 3]. Section 1.1 of this paper provides a concise overview of this method. Reviews of various other modeling methods for radiative heat transfer are reported in [5, 6, 7, 8, 9, 10, 11].

According to [8], the zone method is one of the fastest approaches for analyzing thermal radiation if the exchange areas are known. However, the calculation of direct exchange areas is still a time-consuming and thus limiting factor of the zone method. In fact, it involves integrals with four, five, or six variables [2, 3]. Currently, there is no perspective to compute direct exchange areas in real time. Despite growing computer power and the advent of multi-core systems and parallel computing, the computation of direct exchange areas for general three-dimensional problems with complex geometries is still not feasible within reasonable times. This conclusion may also be drawn from the literature in this field, which is briefly reviewed in Section 1.2. The lack of an efficient method for calculating direct exchange areas is the principal impetus for this work.

The paper is organized as follows: Section 2 demonstrates that the multiple integrals associated with direct exchange areas should not be solved by direct application of numerical quadrature techniques due to singularity problems. Therefore, we explore in Section 3 how coordinate and geometric transformations can avoid these singularities. In Section 4, we validated the effectiveness and accuracy of the method based on benchmark example problems. In a case study, we use the approach in a simulation model of an industrial furnace and compare the simulation results with measurements from the real plant. This demonstrates the applicability of the method to large-scale problems.

1.1. Zone Method

Consider a volume that is filled with participating gas. In this volume, let the straight path of a single ray of thermal radiation be parameterized by the distance coordinate r . The total intensity of the ray at some point r is $I(r)$. From the radiative transfer equation [2, 3], it is known that the total intensity of the ray is attenuated according to

$$I(r_j) = I(r_i)e^{-\bar{r}_{ij}} \quad (1)$$

as it travels from $r = r_i$ to $r = r_j$ through the participating gas. The dimensionless quantity

$$\bar{r}_{ij} = \int_{r_i}^{r_j} K(r)dr \quad (2)$$

with the absorption coefficient $K(r)$ is also known as optical thickness of the path from r_i to r_j . In a gaseous medium where K is constant, K^{-1} is the mean free path of a photon until it is absorbed. In Eq. (1), we have not considered that the total intensity may also increase because of radiative emission of the gas itself. This effect is captured by the term

$$K(r)\frac{\sigma}{\pi}T^4dV, \quad (3)$$

which is the total heat flux emitted by an infinitesimal volume element dV per unit solid angle. T is the local gas temperature and σ is the Stefan-Boltzmann constant. The term $\sigma T^4/\pi$ represents the total intensity of black bodies.

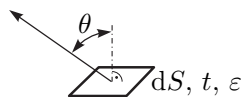


Figure 1. Emergent angle of an emitting surface.

An infinitesimal section dS of a solid, gray, diffuse surface with the temperature t emits the directional total heat flux

$$\varepsilon\frac{\sigma}{\pi}t^4\cos(\theta)dS \quad (4)$$

per unit solid angle. The radiative heat flux depends on the emergent angle $\theta \in [0, \pi/2]$ (cf. Fig. 1) insofar as it is proportional to the projected area $\cos(\theta)dS$ of the emitter. Moreover, it is proportional to the emissivity $\varepsilon \in [0, 1]$, which is a surface property.

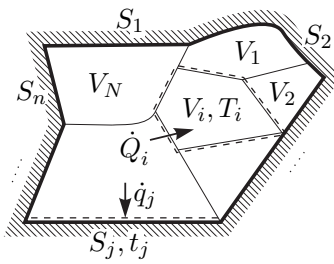


Figure 2. Opaque enclosure filled by participating gas.

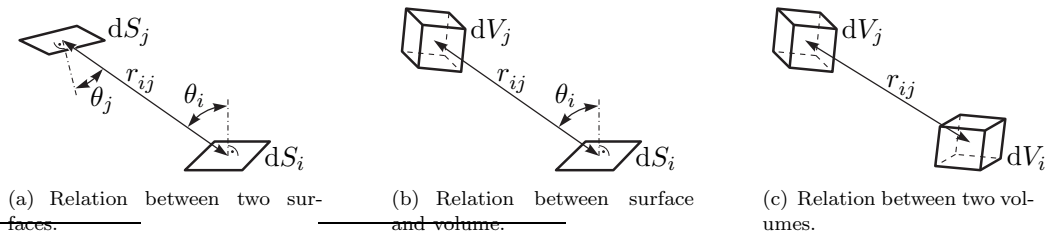


Figure 3. Geometric relation between two infinitesimal zone sections.

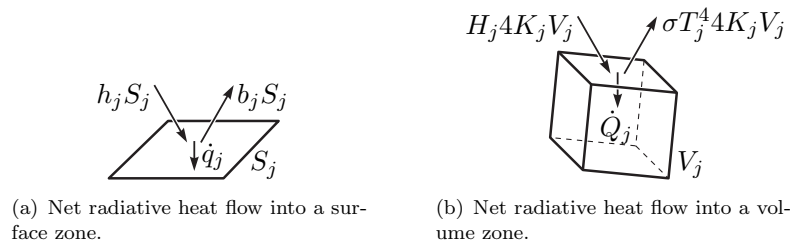


Figure 4. Net radiative heat flows into zones.

We are interested in the heat flows inside an opaque enclosure filled by a participating gaseous medium. The situation is outlined in Fig. 2. For the zone method, the enclosing surface and the internal volume are partitioned into N_S isothermal surface zones and N_V isothermal volume zones, respectively. Then, linear relations between radiative flows diffusely emitted by a zone i (emitter) and the portion of it that is directly absorbed or reflected by the zone j (receiver) can be found. The factors defining these linear relations are called direct exchange areas. They can be computed by integration over all possible rays of thermal radiation traveling from the emitter i through the participating medium directly to the receiver j . Possible rays of thermal radiation are shown in Fig. 3. The geometric path length of these rays is r_{ij} , their optical thickness is \bar{r}_{ij} , and according to (1) their intensity is reduced by the factor $e^{-\bar{r}_{ij}}$ (transmittance).

Throughout the following analysis, we assume that the temperature and the emissivity or the absorption coefficient are uniform within the respective zone. For a surface zone j , we thus have $t = t_j$ and $\varepsilon = \varepsilon_j$. For a volume zone j , we have $T = T_j$ and $K = K_j$.

Assume that $h_j S_j$ is the total radiative heat flow that is incident onto the surface S_j (h_j is known as irradiance). The portion $\varepsilon_j h_j S_j$ of $h_j S_j$ is absorbed by the opaque surface

and the remaining part $(1 - \varepsilon_j)h_j S_j$ is reflected. Let the surface have the temperature t_j so that the emitted radiative heat flow is $\varepsilon_j \sigma t_j^4 S_j$. Thus,

$$b_j S_j = ((1 - \varepsilon_j)h_j + \varepsilon_j \sigma t_j^4) S_j \quad (5)$$

is the total radiative heat flow that departs from the surface S_j (b_j is known as radiosity). As indicated in Fig. 4(a), this yields the net radiative heat flow into the surface

$$\dot{q}_j = (h_j - b_j) S_j = \varepsilon_j (h_j - \sigma t_j^4) S_j. \quad (6)$$

For volume zones, the situation is somewhat simpler because they do not reflect radiation. Assume that $4K_j V_j H_j$ is the radiative heat flow absorbed by a volume V_j . Integrating Eq. (3) over all possible spatial directions (full solid angle, $4\pi \text{sr}$) yields that the volume emits the radiative heat flow $\sigma T_j^4 4K_j V_j$ if T_j is the uniform temperature of the gas in the volume. Consequently, the net radiative heat flow into the volume V_j (cf. Fig. 4(b)) is

$$\dot{Q}_j = (H_j - \sigma T_j^4) 4K_j V_j. \quad (7)$$

The remaining unknowns h_j and H_j can be computed from a radiation balance, i. e., by summing up the heat flows departing from surface and volume zones. Consider first the interacting surface zones S_i and S_j . The portion of $S_j h_j$ that comes directly from S_i is found by integrating over all possible rays of thermal radiation between the two surfaces, i. e.,

$$b_i \underbrace{\int_{S_i} \int_{S_j} \frac{\cos(\theta_i) \cos(\theta_j) e^{-\bar{r}_{ij}}}{\pi r_{ij}^2} dS_j dS_i}_{=: \overline{s_i s_j}}, \quad (8)$$

where $\overline{s_i s_j} \in [0, \min(S_i, S_j)]$ is called surface-surface direct exchange area. Eq. (8) can be deduced by consideration of Fig. 3(a), Eq. (1), Eq. (4), and the fact that dS_j occupies the solid angle $\cos(\theta_j) dS_j / r_{ij}^2$ in the field of view of dS_i .

Next, consider a volume V_i and a surface S_j . The portion of $S_j h_j$ that comes directly from V_i is found by integrating over all possible rays of thermal radiation between the

two zones, i. e.,

$$\sigma T_i^4 \underbrace{\int_{V_i} \int_{S_j} \frac{\cos(\theta_j) K_j e^{-\bar{r}_{ij}}}{\pi r_{ij}^2} dS_j dV_i}_{=: \overline{v_i s_j}}, \quad (9)$$

where $\overline{v_i s_j} \in [0, \min(4K_i V_i, S_j)]$ is called volume-surface direct exchange area. Eq. (9) can be deduced by consideration of Fig. 3(b), Eq. (1), Eq. (3), and the fact that dS_j occupies the solid angle $\cos(\theta_j) dS_j / r_{ij}^2$ in the field of view of dV_i .

In a similar way, consider a surface S_i and a volume V_j . The portion of $4K_j V_j H_j$ that comes directly from S_i is found in the form

$$b_i \underbrace{\int_{S_i} \int_{V_j} \frac{\cos(\theta_i) K_j e^{-\bar{r}_{ij}}}{\pi r_{ij}^2} dV_j dS_i}_{=: \overline{s_i v_j}}, \quad (10)$$

where $\overline{s_i v_j} \in [0, \min(S_i, 4K_j V_j)]$ is called surface-volume direct exchange area. To deduce Eq. (10), consider Fig. 3(b), Eq. (1), Eq. (4), and that dV_j is a sector of a hollow sphere with (infinitesimal) thickness dr and centered at dS_i . Hence, dV_j occupies the solid angle $dV_j / (r_{ij}^2 dr)$ in the field of view of dS_i and absorbs the fraction $K_j dr$ of the radiative heat flow coming from dS_i within this solid angle.

Finally, consider the volumes V_i and V_j . The portion of $4K_j V_j H_j$ that comes directly from V_i is found in the form

$$\sigma T_i^4 \underbrace{\int_{V_i} \int_{V_j} \frac{K_i K_j e^{-\bar{r}_{ij}}}{\pi r_{ij}^2} dV_j dV_i}_{=: \overline{v_i v_j}}, \quad (11)$$

where $\overline{v_i v_j} \in [0, \min(4K_i V_i, 4K_j V_j)]$ is called volume-volume direct exchange area. To deduce Eq. (11), consider Fig. 3(c), Eq. (1), Eq. (3), and that dV_j is a sector of a hollow sphere with (infinitesimal) thickness dr and centered at dV_i . Hence, dV_j occupies the solid angle $dV_j / (r_{ij}^2 dr)$ in the field of view of dV_i and absorbs the fraction $K_j dr$ of the radiative heat flow coming from dV_i within this solid angle.

In (8)–(11), we may use $\bar{r}_{ij} = \infty$ (integrand vanishes) if there is an opaque obstacle between the respective integration points. In Section 2.2, we will formalize the effect of opaque obstacles by an explicit indicator function.

Based on Eqs. (5) and (8)–(11), we can compute the total radiative heat flow

$$S_j h_j = \sum_{i=1}^{N_s} ((1 - \varepsilon_i) h_i + \varepsilon_i \sigma t_i^4) \overline{s_i s_j} + \sum_{i=1}^{N_v} \sigma T_i^4 \overline{v_i s_j} \quad (12)$$

that is incident onto the surface S_j and the total radiative heat flow

$$4K_j V_j H_j = \sum_{i=1}^{N_s} ((1 - \varepsilon_i) h_i + \varepsilon_i \sigma t_i^4) \overline{s_i v_j} + \sum_{i=1}^{N_v} \sigma T_i^4 \overline{v_i v_j} \quad (13)$$

that is absorbed by the volume zone V_j . Elimination of all variables h_j and H_j in Eqs. (6), (7), (12), and (13) yields the desired linear relations between the fourth powers of zone temperatures (t_j^4 and T_j^4) and the net heat flows (\dot{q}_j and \dot{Q}_j) associated with thermal radiation. This concludes the theoretical description of the zone method.

The largest part of the computational effort associated with the zone method is usually caused by the multiple integrals for calculating the direct exchange areas in Eqs. (8)–(11). This calculation requires just knowledge of the geometry and the factors K_j . Hence, it is often done before the evaluation of \dot{q}_j and \dot{Q}_j . If neither the geometry nor the factors K_j change, there is no need for recalculating direct exchange areas.

Direct exchange areas have the unit of area, even if i or j or both are volume zones. The formulae in Eqs. (8)–(11) are also applicable for the case $i = j$. Moreover, they satisfy the reciprocity relations

$$\overline{s_i s_j} = \overline{s_j s_i} \quad (14a)$$

$$\overline{v_i s_j} = \overline{s_j v_i} \quad (14b)$$

$$\overline{v_i v_j} = \overline{v_j v_i} \quad (14c)$$

and the summation rules

$$S_j = \sum_{i=1}^{N_s} \overline{s_i s_j} + \sum_{i=1}^{N_v} \overline{v_i s_j} \quad (15a)$$

$$4K_j V_j = \sum_{i=1}^{N_s} \overline{s_i v_j} + \sum_{i=1}^{N_v} \overline{v_i v_j} \quad (15b)$$

(cf. [2, 3, 10]). These relations can be helpful for validating numerical results of direct exchange areas or for reducing the workload when computing them. When solving the multiple integrals in Eqs. (8)–(11), a considerable difficulty is the singularity associated

with $r_{ij} \rightarrow 0$. This will be further analyzed in Section 2.

1.2. Existing Approaches for Explicit Calculation of Direct Exchange Areas

Numerical values for direct exchange areas in rectangular geometries are given in the form of charts in [12]. Moreover, curve fitting techniques are applied to obtain exponential functions that approximate the given numerical results [10].

In Cartesian coordinates, the length r_{ij} of a ray $\vec{r}_{ij} = \vec{x}_j - \vec{x}_i$ emitted from \vec{x}_i to \vec{x}_j is computed by

$$r_{ij} := |\vec{x}_i - \vec{x}_j| := \sqrt{(x_{i,1} - x_{j,1})^2 + (x_{i,2} - x_{j,2})^2 + (x_{i,3} - x_{j,3})^2} \quad (16)$$

and depends only on the differences $x_{i,1} - x_{j,1}$, $x_{i,2} - x_{j,2}$, and $x_{i,3} - x_{j,3}$. For planar surfaces, $\cos(\theta_i)$ and $\cos(\theta_j)$ also depend only on these differences. If $K_i = K_j = K$, these facts can be utilized for reducing the multiple integrals in Eqs. (8)–(11) to integrals with lower dimensions. This reduced integration scheme was originally proposed by Errku [13]. As demonstrated in [14] for a system with cylindrical coordinates, the scheme saves more than 80 % of the CPU time needed for conventional numerical quadrature. Moreover, it reduces the severity of most singularities which occur if two zones are adjacent or overlapping ($i = j$). In fact, the method described in [14] transfers the singularities to the boundary of the integration domain but does not remove them. A similar reduced integration method for direct exchange areas of a cylindrical enclosure is described in [15]. The methods described in [13, 14, 15] do not consider the mutual visibility between integration points, i.e., it is not checked whether an opaque obstacle separates the integration points. The methods are thus only applicable to convex geometries. A mixed approach is reported in [16], where direct exchange areas of adjacent or overlapping zones are calculated by means of the finite volume method [17] to circumvent the problem of singularities. All other direct exchange areas are approximately computed by a midpoint integration scheme [3]. In this case, the integrands in Eqs. (8)–(11) are only evaluated at the barycenters of the zones. The accuracy of the method is improved, if the zones have small optical thicknesses and large optical distances. In [18], the spatial discretization is refined by further division of zones and application of the midpoint integration scheme to the refined grid. To circumvent problems with singularities at overlapping zones, vanishing center-to-center distances are either replaced by a semi-empirical positive approximation or the respective direct exchange area is set to zero.

Another reduced integration scheme for direct exchange areas is proposed in [19]. In-

integrals over a volume zone V_i are replaced by two-dimensional integrals over the boundaries surrounding the volume zone. In fact, only those sections of the boundary of V_i that are directly visible to the corresponding zone (S_j or V_j) enter the integral. Therefore, Eqs. (9)–(11) for surface-volume and volume-volume direct exchange areas are simplified to integrals with only four variables. In [19], the absorbance factor $1 - e^{-Kr_i}$, where K is constant and r_i is the geometric length of the ray inside the volume V_i , is multiplied to the integrand to capture that the fraction e^{-Kr_i} of the total intensity of the respective ray passes through the volume (cf. Eq. (1)). A similar approach is presented in [20], but there the surface integrals that replace the volume integrals over V_i , are evaluated on the whole boundary of V_i . It is not clear, how the problem of singularities occurring in the direct exchange areas of adjacent or overlapping zones is tackled in [19] and [20].

A volume zone V_i entails a singular integral kernel when evaluating $\overline{v_i v_i}$. Similar problems occur in the evaluation of the other direct exchange areas defined in Eqs. (8)–(11). The problem of singularities is usually avoided in the literature by introducing approximations of the respective direct exchange areas. A drawback of this approach is the possible accumulation of unknown approximation errors and the prevention of a rigorous mathematical analysis. The approach may, for instance, cause a violation of the summation rules Eq. (15) (cf. [14]).

1.3. *Avoiding Singular Integral Kernels in the Calculation of Direct Exchange Areas*

In this work, we resolve the problem of singular kernels by applying certain coordinate transformations which lead to smooth integral kernels that can be evaluated by standard Gaussian quadrature. Due to strong similarities between the singular kernels in Eqs. (8)–(11) to those arising in boundary element methods, we adapt the methods proposed in [21]. The basic ideas are the following: Since the singularity is present at the points which satisfy $\vec{x}_i = \vec{x}_j$, we split the integration domain around these singular points into several subdomains. After changing the order of integration in these subdomains, the application of appropriate Duffy transformations removes the singularities, i.e., the resulting integral kernel is smooth. Intuitively, this is achieved by stretching the points (lines) on which the singularity is present, to lines (faces). Hence, we conceptually distribute the singularity on a larger domain and thus remove it. According to the Fubini theorem, this approach results in multiple 1D line integrals which are approximated by Gaussian quadrature. Due to the benign numerical properties of the transformed integral kernels, it suffices to use only a small number of quadrature points. Hence, it requires only low computational effort to achieve highly accurate results.

The advantages of the proposed method are manifold: It allows quite general integral kernels, which can be used, e.g., in the case of non-homogeneous gas-distributions or in the case of opaque (surfaces) obstacles within the volume zone. The approach gives reliable results for direct exchange areas in the case of adjacent zones (surface-surface $\overline{s_i s_j}$, volume-surface $\overline{v_i s_j}$, and volume-volume $\overline{v_i v_j}$ with $i \neq j$) and even in the case of self-interacting zones (surface-surface $\overline{s_i s_i}$ and volume-volume $\overline{v_i v_i}$). Moreover, the method allows for a thorough mathematical analysis which guarantees exponential accuracy of the results. For the ease of presentation, we consider axis-parallel volume and surface zones only. However, the principal ideas transfer to more complex situations.

2. DESCRIPTION OF THE PROBLEM AND SINGULARITIES

To demonstrate the difficulties associated with singular integral kernels, we consider the volume-volume direct exchange areas from Eq. (11), which can be written as

$$\overline{v_i v_j} = \int_{V_i} \int_{V_j} k(\vec{x}_i, \vec{x}_j) dV_i dV_j \quad (17)$$

where $\vec{x}_i \in V_i$ and $\vec{x}_j \in V_j$ are the integration variables and the integrand is

$$k(\vec{x}_i, \vec{x}_j) := \frac{1}{|\vec{x}_j - \vec{x}_i|^2} K_i K_j \frac{e^{-\tau_{ij}}}{\pi}, \quad (18)$$

see Eq. (16) for the definition of $|\vec{x}_j - \vec{x}_i|$. Note that the integrand is smooth for all $\vec{x}_i \neq \vec{x}_j$ and exhibits singularities for $\vec{x}_i = \vec{x}_j$. The latter requires that V_i and V_j overlap or touch each other. Despite these singularities, the inner integral in Eq. (17) exists as a proper integral because the integration domain V_j is 3-dimensional but the integrand $k(\cdot, \cdot)$ is only singular of order 2. In particular, the Fubini theorem applies and allows to interchange the order of integration in Eq. (17).

In numerical computations, the possible singularities at $\vec{x}_i = \vec{x}_j$ impair the accuracy of quadrature formulas like Gaussian quadrature (cf. Eq. (19)) or may even prohibit their use. In Section 4.1, we present a numerical example which demonstrates that Gaussian quadrature may lead to unreliable results for tractable quadrature orders.

2.1. Geometry

Suppose that the volume zones V_i are axis-parallel cuboids, i.e., there exists a vector $\vec{x}^i = (x_1^i, x_2^i, x_3^i) \in \mathbb{R}^3$ and side lengths $d_1^i, d_2^i, d_3^i > 0$ with

$$V_i := [x_1^i, x_1^i + d_1^i] \times [x_2^i, x_2^i + d_2^i] \times [x_3^i, x_3^i + d_3^i].$$

Note that \vec{x}^i and the side lengths characterize the volume zone V_i while $\vec{x}_i \in V_i$ is the integration variable, e.g., in Eq. (17). Analogously, suppose that surface zones S_i are axis-parallel rectangles that are obtained by setting one of the above side lengths to zero, i.e.,

$$S_i := [x_1^i, x_1^i + d_1^i] \times [x_2^i, x_2^i + d_2^i] \times \{x_3^i\} \quad \text{or}$$

$$S_i := [x_1^i, x_1^i + d_1^i] \times \{x_2^i\} \times [x_3^i, x_3^i + d_3^i] \quad \text{or}$$

$$S_i := \{x_1^i\} \times [x_2^i, x_2^i + d_2^i] \times [x_3^i, x_3^i + d_3^i].$$

For the coordinate transformations below, we use the unit cube

$$V_{\text{ref}} := [0, 1] \times [0, 1] \times [0, 1]$$

as a reference volume. Coordinates on the reference volume are denoted by Greek letters, e.g., $\vec{\alpha} = (\alpha_1, \alpha_2, \alpha_3) \in V_{\text{ref}}$. For all volume zones V_i , there exists a transformation $\Lambda_i : V_{\text{ref}} \rightarrow V_i$, given by

$$\Lambda_i(\vec{\alpha}) := (x_1^i + \alpha_1 d_1^i, x_2^i + \alpha_2 d_2^i, x_3^i + \alpha_3 d_3^i).$$

On the reference volume, the integral of a continuous integrand f can be approximated by use of the Fubini theorem and iterated 1D Gaussian quadrature, i.e.,

$$\begin{aligned} \int_{V_{\text{ref}}} f(\vec{\alpha}) \, dV_{\text{ref}} &= \int_0^1 \int_0^1 \int_0^1 f(\alpha_1, \alpha_2, \alpha_3) \, d\alpha_1 \, d\alpha_2 \, d\alpha_3 \\ &\approx \sum_{i=0}^M \sum_{j=0}^M \sum_{k=0}^M w_i w_j w_k f(s_i, s_j, s_k), \end{aligned} \tag{19}$$

where s_1, \dots, s_M denote the evaluation points and w_1, \dots, w_M denote the corresponding weights for the 1D Gaussian quadrature rule of order M on the interval $[0, 1]$. If f is sufficiently smooth, the approximation error follows the exponential decay $\exp(-M)$.

2.2. Visibility

In more complex geometries (enclosures), a ray emitted at the point $\vec{x}_i \in V_i$ and sent along the direction $\vec{r}_{ij} = \vec{x}_j - \vec{x}_i$ with $\vec{x}_j \in V_j$ might hit an opaque obstacle before it arrives at \vec{x}_j . Hence, this ray does not contribute to the direct exchange area computed in Eq. (17). To capture this effect, we extend the kernel $k(\vec{x}_i, \vec{x}_j)$ from Eq. (18) by an indicator function $\text{vis}(\vec{x}_i, \vec{x}_j) \in \{0, 1\}$ to get

$$k(\vec{x}_i, \vec{x}_j) := \frac{1}{|\vec{x}_j - \vec{x}_i|^2} K_i K_j \frac{e^{-\vec{r}_{ij}}}{\pi} \text{vis}(\vec{x}_i, \vec{x}_j). \quad (20)$$

The indicator function satisfies $\text{vis}(\vec{x}_i, \vec{x}_j) = 1$ if there is no obstacle between $\vec{x}_i \in V_i$ and $\vec{x}_j \in V_j$ and $\text{vis}(\vec{x}_i, \vec{x}_j) = 0$ otherwise. At first glance, the evaluation of $\text{vis}(\vec{x}_i, \vec{x}_j)$ can be a challenge in the implementation of complex geometries. However, note that opaque obstacles are represented by surface zones S_k .

For geometries with few surface zones (e.g., $N_S = 500$ zones or less), a tractable way is to loop through a list of all surface zones S_k and to check if \vec{r}_{ij} intersects S_k . However, when more zones are involved, a hierarchical approach is more efficient. To that end, a preprocessing step groups the surface zones which lie close to each other, via so-called bounding boxes. A bounding box is the smallest axis-parallel cuboid which contains all surface zones of the particular group. This preprocessing step is described in the following. It is closely related to the hierarchical concept of the fast multipole method [22, 23]. For the general concept of bounding boxes, we also refer, e.g., to [24] in the context of hierarchical matrices.

$B_\alpha = \text{boundingBox}(\mathcal{S}_\alpha);$

if $|\mathcal{S}_\alpha| > N_{\text{cut}}$ {
 $[\mathcal{S}_{(\alpha,0)}, \dots, \mathcal{S}_{(\alpha,7)}] = \text{divideBoundingBox}(\mathcal{S}_\alpha, B_\alpha);$

for $n = 0$ to 7 {
 $S((\alpha, n));$
 $\}$
 $\}$

Listing 1 Function $S(\alpha)$ for generating a hierarchy of bounding boxes.

Let $\mathcal{S}_{(0)}$ be the set of barycenters of all surface zones S_k , $k = 1, \dots, N_S$. The bounding boxes are build by a recursive algorithm by using the function $S(\alpha)$ which is outlined in Listing 1. Here, α denotes a tuple. The function $\text{boundingBox}(\mathcal{S}_\alpha)$ computes a bounding box B_α that contains all surface zones S with barycenters in \mathcal{S}_α . Moreover, the function $\text{divideBoundingBox}(\mathcal{S}_\alpha, B_\alpha)$ divides B_α geometrically into eight boxes of equal size and computes the corresponding disjoint subsets of barycenters $\mathcal{S}_{(\alpha,n)}$, $n = 0, \dots, 7$. Starting with $S((0))$, a hierarchy of bounding boxes with corresponding groups of surface zones

is generated. A useful value for the cut-off value N_{cut} is $N_{\text{cut}} = 10$. Note that bounding boxes may overlap even at the same hierarchical level.

The preprocessing step produces a number of nested bounding boxes, $B_{(0)} \supset B_{(0,n_1)} \supset B_{(0,n_1,n_2)} \supset \dots$ for $n_1, n_2, \dots \in \{0, \dots, 7\}$. Clearly, if a bounding box $B_{(0,n_1,\dots,n_k)}$ is not partitioned into smaller bounding boxes, it contains less than or equal N_{cut} surface zones. If the surface zones are approximately (within one order of magnitude) uniformly distributed and if the distance between their barycenters coincides roughly with their diameter, the maximal depth (i.e., the maximal number $k \in \mathbb{N}$ such that a box $B_{(0,n_1,\dots,n_k)}$ exists) satisfies $k \approx \log_8(N_S)$, where N_S is total number of surface zones. This is due to the fact that each box $B_{(0,n_1,\dots,n_k)}$ contains approximately 1/8 of the surface zones of its parent box $B_{(0,n_1,\dots,n_{k-1})}$. We note that k depends also on N_{cut} which is, however, fixed.

```

if intersectsBox( $\vec{r}_{ij}, B_\alpha$ ) {
  if  $|\mathcal{S}_\alpha| > N_{\text{cut}}$  {
    for  $n = 0$  to 7 {
      C( $(\alpha, n)$ );
    }
  }
  else {
    for each  $S$  with barycenter in  $\mathcal{S}_\alpha$  {
      if intersectsZone( $\vec{r}_{ij}, S_n$ ) {
        vis = 0;
        quit;
      }
    }
  }
}

```

Listing 2 Function $C(\alpha)$ for computing the visibility $\text{vis}(\vec{x}_i, \vec{x}_j)$ based on the hierarchy of bounding boxes.

To evaluate $\text{vis}(\vec{x}_i, \vec{x}_j)$, again a recursive algorithm is applied using the function $C(\alpha)$ outlined in Listing 2. The variable vis is initialized by the value 1 and the vector $\vec{r}_{ij} := \vec{x}_j - \vec{x}_i$ denotes the ray from \vec{x}_i to \vec{x}_j . The function $\text{intersectsBox}(\vec{r}_{ij}, B_\alpha)$ checks if \vec{r}_{ij} intersects the bounding box B_α and the function $\text{intersectsZone}(\vec{r}_{ij}, S_n)$ checks if \vec{r}_{ij} intersects the surface zone S . Evaluation of $C((0))$ yields the visibility, i.e., $\text{vis}(\vec{x}_i, \vec{x}_j) = \text{vis}$.

The precise complexity of the outlined algorithm depends on the distribution and size of the surface zones in an intricate way. However, we may give a heuristic argument for an enclosure in the form of a unit cube $[0, 1]^3$: We suppose that, for a hierarchical level k , there exist $\leq 8^k$ bounding boxes with an edge length of approximately 2^{-k} such that the boxes of the same level overlap at most by half of their edge length, i.e., a cube is essentially divided into 8 cubes. An axis-parallel ray \vec{r}_{ij} with length (at most) $r_{ij} = 1$ will intersect at most $8r_{ij}/2^{-k} \approx 2^k$ boxes of level k . (A ray that is not axis-parallel might intersect more boxes but the number of intersections has still the order of magnitude

2^k .) Hence, the total number of intersected boxes M can be estimated by

$$M \lesssim \sum_{k=0}^{\log_8(N_S)} 2^k \leq 2^{1+\log_8(N_S)} - 1 \approx N_S^{1/3}.$$

This means that the function $\mathcal{C}(\alpha)$ is called approximately $N_S^{1/3}$ times, which is a significant improvement compared to the direct approach with approximately N_S operations.

3. INTEGRATION WITH TRANSFORMED COORDINATES

In this section, we present coordinate transformations which lead to smooth kernels. We discuss only the transformations used for the volume-volume case, i.e., $\overline{v_i v_j}$, because this is the most complex situation. The other cases $\overline{v_i s_j}$ and $\overline{s_i s_j}$ can be analyzed and treated in a similar manner.

3.1. Volume-Volume Direct Exchange Areas

We consider the computation of the integral Eq. (17) with $k(\vec{x}_i, \vec{x}_j)$ defined in Eq. (20).

We can distinguish between the cases:

- $V_i = V_j$ (Section 3.1.1),
- V_i and V_j share a joint face,
- V_i and V_j share a joint edge,
- V_i and V_j share a joint vertex,
- the minimum distance between V_i and V_j is greater than zero, i.e., $V_i \cap V_j = \emptyset$ (Section 3.1.2).

We describe the method only for the first and the last case. The case $V_i = V_j$ is interesting because it entails the most severe singularity in the integral kernel. The case where V_i and V_j are disjoint volumes is shown because it does not entail any singularities. The other cases follow with similar techniques.

3.1.1. Identical Volumes

For this section, we have to abandon the notation dV_i in favor of the rigorous notation $d\vec{x}_i$, which specifies the integration variable \vec{x}_i . The integration domain is V_i .

Let $V_i = V_j = [x_1^i, x_1^i + d_1^i] \times [x_2^i, x_2^i + d_2^i] \times [x_3^i, x_3^i + d_3^i]$ be an arbitrary axis-parallel cuboid with corresponding transformations $\Lambda_i = \Lambda_j$ from Section 2.1. Substitution of Λ_i

transfers the integral Eq. (17) to the reference volume, i.e.,

$$\overline{v_i v_i} = \int_{V_i} \int_{V_j} k(\vec{x}_i, \vec{x}_j) d\vec{x}_i d\vec{x}_j = |V_i|^2 \int_{V_{\text{ref}}} \int_{V_{\text{ref}}} k(\Lambda_i(\vec{\alpha}), \Lambda_i(\vec{\beta})) d\vec{\beta} d\vec{\alpha}. \quad (21)$$

With the relative coordinates $\vec{\gamma} := \vec{\beta} - \vec{\alpha} = (\gamma_1, \gamma_2, \gamma_3)$, we write

$$g(\vec{\gamma}) := \frac{\exp(-K_i |d_1^i \gamma_1, d_2^i \gamma_2, d_3^i \gamma_3|)}{|d_1^i \gamma_1, d_2^i \gamma_2, d_3^i \gamma_3|^2}, \quad f(\vec{\alpha}, \vec{\beta}) := |V_i|^2 \frac{K_i^2}{\pi} \text{vis}(\Lambda_i(\vec{\alpha}), \Lambda_i(\vec{\beta})). \quad (22)$$

We define the transformed integral kernel

$$\tilde{k}(\vec{\alpha}, \vec{\beta}) := |V_i|^2 k(\Lambda_i(\vec{\alpha}), \Lambda_i(\vec{\beta})) = g(\vec{\beta} - \vec{\alpha}) f(\vec{\alpha}, \vec{\beta}). \quad (23)$$

Note that g contains the singular behavior of the integral kernel. Moreover, g and f are symmetric in the sense that $g(\vec{\gamma}) = g(-\vec{\gamma})$ and $f(\vec{\alpha}, \vec{\beta}) = f(\vec{\beta}, \vec{\alpha})$, respectively. As outlined in Fig. 5, we first substitute $\vec{\beta} = \vec{\alpha} + \vec{\gamma}$. Then,

$$\overline{v_i v_i} = \int_{V_{\text{ref}}} \int_{(V_{\text{ref}} - \vec{\alpha})} \tilde{k}(\vec{\alpha}, \vec{\alpha} + \vec{\gamma}) d\vec{\gamma} d\vec{\alpha}, \quad (24)$$

where $V_{\text{ref}} - \vec{\alpha}$ denotes the set V_{ref} shifted by $-\vec{\alpha}$. Clearly, we have a singular behavior as $\vec{\gamma} \rightarrow (0, 0, 0)$. This is why we split the 6-dimensional integration domain into eight non-overlapping subdomains around $\vec{\gamma} = (0, 0, 0)$ (see Fig. 5). These domains are given by

$$D_1 = \left\{ \begin{array}{l} \vec{\alpha} \in [0, 1]^3 \\ \gamma_1 \in [-\alpha_1, 0] \\ \gamma_2 \in [-\alpha_2, 0] \\ \gamma_3 \in [-\alpha_3, 0] \end{array} \right\}, \quad D_2 = \left\{ \begin{array}{l} \vec{\alpha} \in [0, 1]^3 \\ \gamma_1 \in [0, 1 - \alpha_1] \\ \gamma_2 \in [0, 1 - \alpha_2] \\ \gamma_3 \in [0, 1 - \alpha_3] \end{array} \right\},$$

$$D_3 = \left\{ \begin{array}{l} \vec{\alpha} \in [0, 1]^3 \\ \gamma_1 \in [-\alpha_1, 0] \\ \gamma_2 \in [0, 1 - \alpha_2] \\ \gamma_3 \in [-\alpha_3, 0] \end{array} \right\}, \quad D_4 = \left\{ \begin{array}{l} \vec{\alpha} \in [0, 1]^3 \\ \gamma_1 \in [0, 1 - \alpha_1] \\ \gamma_2 \in [-\alpha_2, 0] \\ \gamma_3 \in [0, 1 - \alpha_3] \end{array} \right\},$$

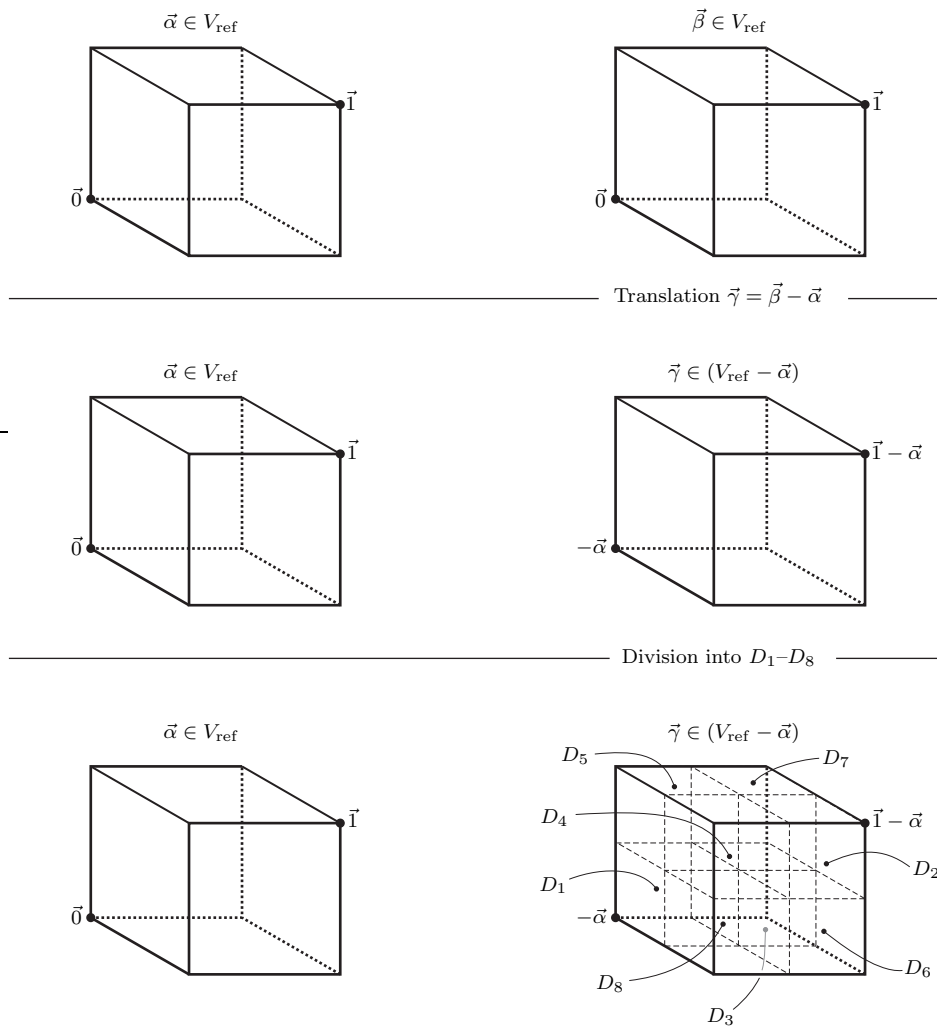


Figure 5. First coordinate transformation and division of integration domain.

$$D_5 = \left\{ \begin{array}{l} \vec{\alpha} \in [0, 1]^3 \\ \gamma_1 \in [-\alpha_1, 0] \\ \gamma_2 \in [-\alpha_2, 0] \\ \gamma_3 \in [0, 1 - \alpha_3] \end{array} \right\}, \quad D_6 = \left\{ \begin{array}{l} \vec{\alpha} \in [0, 1]^3 \\ \gamma_1 \in [0, 1 - \alpha_1] \\ \gamma_2 \in [0, 1 - \alpha_2] \\ \gamma_3 \in [-\alpha_3, 0] \end{array} \right\}, \\
 D_7 = \left\{ \begin{array}{l} \vec{\alpha} \in [0, 1]^3 \\ \gamma_1 \in [-\alpha_1, 0] \\ \gamma_2 \in [0, 1 - \alpha_2] \\ \gamma_3 \in [0, 1 - \alpha_3] \end{array} \right\}, \quad D_8 = \left\{ \begin{array}{l} \vec{\alpha} \in [0, 1]^3 \\ \gamma_1 \in [0, 1 - \alpha_1] \\ \gamma_2 \in [-\alpha_2, 0] \\ \gamma_3 \in [-\alpha_3, 0] \end{array} \right\}.$$

and satisfy $\bigcup_{j=1}^8 D_j = V_{\text{ref}} \times (V_{\text{ref}} - \vec{\alpha})$. Thus, the integral $\overline{v_i v_i}$ changes to

$$\overline{v_i v_i} = \sum_{j=1}^8 \int_{D_j} \tilde{k}(\vec{\alpha}, \vec{\alpha} + \vec{\gamma}) d\vec{\gamma} d\vec{\alpha}. \quad (25)$$

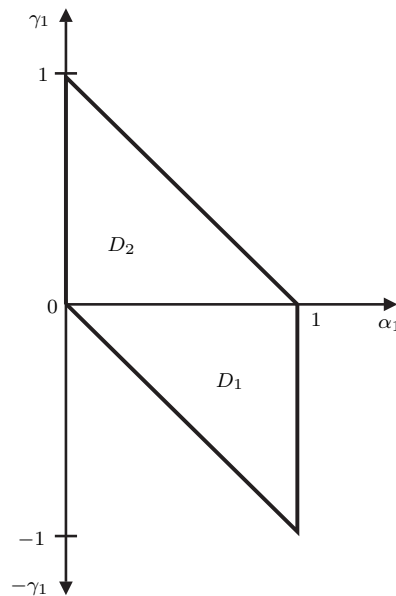


Figure 6. Parametrization of the integration domain $V_{\text{ref}} \times (V_{\text{ref}} - \vec{\alpha})$ required for changing the order of integration, where only the first components (γ_1, α_1) are visualized.

The domains D_1 and D_2 (cf. Fig. 6) can equivalently be written as

$$D_1 = \left\{ \begin{array}{l} \vec{\gamma} \in [-1, 0]^3 \\ \alpha_1 \in [-\gamma_1, 1] \\ \alpha_2 \in [-\gamma_2, 1] \\ \alpha_3 \in [-\gamma_3, 1] \end{array} \right\}, \quad D_2 = \left\{ \begin{array}{l} \vec{\gamma} \in [0, 1]^3 \\ \alpha_1 \in [0, 1 - \gamma_1] \\ \alpha_2 \in [0, 1 - \gamma_2] \\ \alpha_3 \in [0, 1 - \gamma_3] \end{array} \right\}. \quad (26)$$

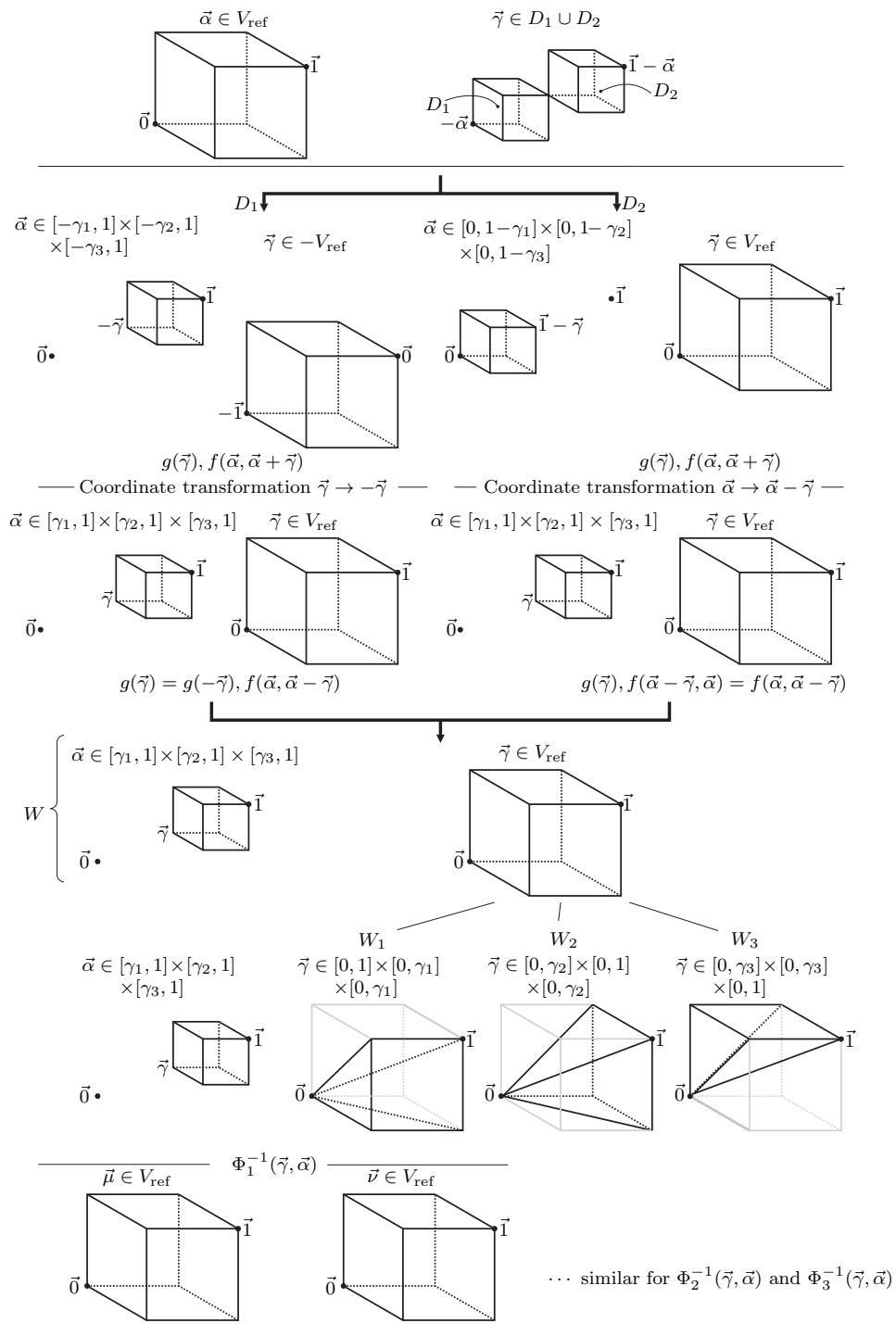


Figure 7. Coordinate transformations.

With symmetry of g and f , the coordinate transformations $\bar{\gamma} \rightarrow -\bar{\gamma}$ and $\bar{\alpha} \rightarrow \bar{\alpha} - \bar{\gamma}$

are applied to D_1 and D_2 , respectively (cf. Fig. 7). We get

$$\int_{D_1 \cup D_2} \tilde{k}(\vec{\alpha}, \vec{\alpha} + \vec{\gamma}) d\vec{\gamma} d\vec{\alpha} = 2 \int_{[0,1]^3} g(\vec{\gamma}) \int_{\gamma_1}^1 \int_{\gamma_2}^1 \int_{\gamma_3}^1 f(\vec{\alpha}, \vec{\alpha} - \vec{\gamma}) d\alpha_1 d\alpha_2 d\alpha_3 d\vec{\gamma}, \quad (27)$$

as indicated in Fig. 7. In this way, we have transformed the integration over $D_1 \cup D_2$ into an integration over

$$W = \left\{ \begin{array}{l} \vec{\gamma} \in [0, 1]^3 \\ \alpha_1 \in [\gamma_1, 1] \\ \alpha_2 \in [\gamma_2, 1] \\ \alpha_3 \in [\gamma_3, 1] \end{array} \right\}. \quad (28)$$

Still, the integrand exhibits a singular behavior for $\vec{\gamma} = (0, 0, 0)$. To get rid of this singularity, we will use a special Duffy transformation. To that end, we split the reference volume $V_{\text{ref}} = [0, 1]^3$ for $\vec{\gamma}$ into three subdomains (pyramides shown in Fig. 7). This gives the non-overlapping integration domains

$$W_1 = \left\{ \begin{array}{l} \gamma_1 \in [0, 1] \\ \gamma_2 \in [0, \gamma_1] \\ \gamma_3 \in [0, \gamma_1] \\ \alpha_1 \in [\gamma_1, 1] \\ \alpha_2 \in [\gamma_2, 1] \\ \alpha_3 \in [\gamma_3, 1] \end{array} \right\}, W_2 = \left\{ \begin{array}{l} \gamma_1 \in [0, \gamma_2] \\ \gamma_2 \in [0, 1] \\ \gamma_3 \in [0, \gamma_2] \\ \alpha_1 \in [\gamma_1, 1] \\ \alpha_2 \in [\gamma_2, 1] \\ \alpha_3 \in [\gamma_3, 1] \end{array} \right\}, W_3 = \left\{ \begin{array}{l} \gamma_1 \in [0, \gamma_3] \\ \gamma_2 \in [0, \gamma_3] \\ \gamma_3 \in [0, 1] \\ \alpha_1 \in [\gamma_1, 1] \\ \alpha_2 \in [\gamma_2, 1] \\ \alpha_3 \in [\gamma_3, 1] \end{array} \right\}, \quad (29)$$

which satisfy $W = W_1 \cup W_2 \cup W_3$. Each of these subdomains will then be transformed back to the reference volume V_{ref} by a special Duffy transformation. Moreover, we will also transform the volume $[\gamma_1, 1] \times [\gamma_2, 1] \times [\gamma_3, 1]$ to V_{ref} .

Let Φ_j with $j = 1, 2, 3$ denote the functions which transform $V_{\text{ref}} \times V_{\text{ref}} = [0, 1]^6$ into the domains W_j . The meaning of Φ_1 is indicated in Fig. 7. With $\vec{\mu} = (\mu_1, \mu_2, \mu_3) \in V_{\text{ref}}$ and $\vec{\nu} = (\nu_1, \nu_2, \nu_3) \in V_{\text{ref}}$, the functions Φ_j are given by

$$\Phi_1(\vec{\mu}, \vec{\nu}) = (\mu_1, \mu_1\mu_2, \mu_1\mu_3, \mu_1 + \nu_1(1 - \mu_1), \mu_1\mu_2 + \nu_2(1 - \mu_1\mu_2), \mu_1\mu_3 + \nu_3(1 - \mu_1\mu_3)),$$

$$\Phi_2(\vec{\mu}, \vec{\nu}) = (\mu_1\mu_2, \mu_2, \mu_2\mu_3, \mu_1\mu_2 + \nu_1(1 - \mu_1\mu_2), \mu_2 + \nu_2(1 - \mu_2), \mu_2\mu_3 + \nu_3(1 - \mu_2\mu_3)),$$

$$\Phi_3(\vec{\mu}, \vec{\nu}) = (\mu_1\mu_3, \mu_2\mu_3, \mu_3, \mu_1\mu_3 + \nu_1(1 - \mu_1\mu_3), \mu_2\mu_3 + \nu_2(1 - \mu_2\mu_3), \mu_3 + \nu_3(1 - \mu_3)),$$

The corresponding Jacobian determinants are

$$|\det(\nabla\Phi_1(\vec{\mu}, \vec{\nu}))| = \mu_1^2(1 - \mu_1)(1 - \mu_1\mu_2)(1 - \mu_1\mu_3), \quad (30a)$$

$$|\det(\nabla\Phi_2(\vec{\mu}, \vec{\nu}))| = \mu_2^2(1 - \mu_1\mu_2)(1 - \mu_2)(1 - \mu_2\mu_3), \quad (30b)$$

$$|\det(\nabla\Phi_3(\vec{\mu}, \vec{\nu}))| = \mu_3^2(1 - \mu_1\mu_3)(1 - \mu_2\mu_3)(1 - \mu_3). \quad (30c)$$

According to the transformation theorem and the Fubini theorem, Eq. (27) can be rewritten in the form

$$\begin{aligned} \int_{D_1 \cup D_2} \tilde{k}(\vec{\alpha}, \vec{\alpha} + \vec{\gamma}) d\vec{\gamma} d\vec{\alpha} &= 2 \sum_{j=1}^3 \int_{W_j} \tilde{k}(\vec{\alpha}, \vec{\alpha} - \vec{\gamma}) d\vec{\gamma} d\vec{\alpha} \\ &= 2 \sum_{j=1}^3 \int_{[0,1]^6} \tilde{k}(\Phi_j(\vec{\mu}, \vec{\nu})_{4,5,6}, \Phi_j(\vec{\mu}, \vec{\nu})_{4,5,6} - \Phi_j(\vec{\mu}, \vec{\nu})_{1,2,3}) |\det(\nabla\Phi_j(\vec{\mu}, \vec{\nu}))| d\vec{\mu} d\vec{\nu}. \end{aligned} \quad (31)$$

Note that the first three components $\Phi_i(\vec{\mu}, \vec{\nu})_{1,2,3}$ of $\Phi_i(\vec{\mu}, \vec{\nu})$ map to the variable $\vec{\gamma}$ and the second three components $\Phi_i(\vec{\mu}, \vec{\nu})_{4,5,6}$ of $\Phi_i(\vec{\mu}, \vec{\nu})$ map to the variable $\vec{\alpha}$. It remains to analyze the singularity of the integrand in Eq. (31). We consider the singular part $g(\vec{\gamma})$ from Eq. (27) and multiply it with the determinant of the transformations. This leads to

$$\begin{aligned} g(\Phi_1(\vec{\mu}, \vec{\nu})_{1,2,3}) |\det(\nabla\Phi_1(\vec{\mu}, \vec{\nu}))| \\ &= \frac{\exp(-K|(d_1^i \mu_1, d_2^i \mu_1 \mu_2, d_3^i \mu_1 \mu_3)|)}{|(d_1^i \mu_1, d_2^i \mu_1 \mu_2, d_3^i \mu_1 \mu_3)|^2} \mu_1^2 (1 - \mu_1)(1 - \mu_1 \mu_2)(1 - \mu_1 \mu_3) \\ &= \frac{\exp(-K|(d_1^i \mu_1, d_2^i \mu_1 \mu_2, d_3^i \mu_1 \mu_3)|)}{|(d_1^i, d_2^i \mu_2, d_3^i \mu_3)|^2} (1 - \mu_1)(1 - \mu_1 \mu_2)(1 - \mu_1 \mu_3) =: g_1(\vec{\mu}) \text{ for } \mu_1 > 0. \end{aligned}$$

For Φ_2 and Φ_3 , we proceed analogously and get

$$\begin{aligned} g(\Phi_2(\vec{\mu}, \vec{\nu})_{1,2,3}) |\det(\nabla\Phi_2(\vec{\mu}, \vec{\nu}))| \\ &= \frac{\exp(-K|(d_1^i \mu_1 \mu_2, d_2^i \mu_2, d_3^i \mu_2 \mu_3)|)}{|(d_1^i \mu_1, d_2^i, d_3^i \mu_3)|^2} (1 - \mu_1 \mu_2)(1 - \mu_2)(1 - \mu_2 \mu_3) =: g_2(\vec{\mu}) \text{ for } \mu_2 > 0, \\ g(\Phi_3(\vec{\mu}, \vec{\nu})_{1,2,3}) |\det(\nabla\Phi_3(\vec{\mu}, \vec{\nu}))| \\ &= \frac{\exp(-K|(d_1^i \mu_1 \mu_3, d_2^i \mu_2 \mu_3, d_3^i \mu_3)|)}{|(d_1^i \mu_1, d_2^i \mu_2, d_3^i)|^2} (1 - \mu_1 \mu_3)(1 - \mu_2 \mu_3)(1 - \mu_3) =: g_3(\vec{\mu}) \text{ for } \mu_3 > 0. \end{aligned}$$

Note that the functions $g_1(\vec{\mu})$, $g_2(\vec{\mu})$, and $g_3(\vec{\mu})$ are smooth with respect to $\vec{\mu} \in V_{\text{ref}}$ because the denominator is strictly positive, i.e., the singularity vanishes by multiplying $g(\cdot)$ with the Jacobian determinants from Eq. (30).

Next, we transform the function $f(\vec{\alpha}, \vec{\alpha} - \vec{\gamma})$ from Eq. (27) by means of the Φ_k . For a compact notation, we define the functions f_1^k by

$$f_1^k(\vec{\mu}, \vec{\nu}) := f(\Phi_k(\vec{\mu}, \vec{\nu})_{4,5,6}, \Phi_k(\vec{\mu}, \vec{\nu})_{4,5,6} - \Phi_k(\vec{\mu}, \vec{\nu})_{1,2,3}).$$

For the remaining domains $D_3 \cup D_4$, $D_5 \cup D_6$, and $D_7 \cup D_8$ we proceed similarly. The functions $g_k(\cdot)$ are the same for the other domains but the functions f_1^k differ slightly. We use the notation f_2^k for the case $D_3 \cup D_4$, f_3^k for $D_5 \cup D_6$, and f_4^k for $D_7 \cup D_8$.

Finally, the integral from Eq. (25) becomes

$$\overline{v_i v_i} = \sum_{j=1}^8 \int_{D_j} \tilde{k}(\vec{\alpha}, \vec{\alpha} + \vec{\gamma}) d\vec{\gamma} d\vec{\alpha} = 2 \int_{V_{\text{ref}}} \sum_{k=1}^3 g_k(\vec{\mu}) \int_{V_{\text{ref}}} \sum_{\ell=1}^4 f_\ell^k(\vec{\mu}, \vec{\nu}) d\vec{\nu} d\vec{\mu}, \quad (32)$$

with g_k being smooth. However, the functions f_ℓ^k are in general not analytic because $f(\vec{\alpha}, \vec{\beta})$ contains the non-analytic factor $\text{vis}(\Lambda_i(\vec{\alpha}), \Lambda_j(\vec{\beta})) \in \{0, 1\}$ (cf. Eq. (22)). For the special case $\text{vis} \equiv 1$, Eq. (32) simplifies to

$$\overline{v_i v_i} = \frac{8|V_i|^2 K_i^2}{\pi} \int_{V_{\text{ref}}} \sum_{k=1}^3 g_k(\vec{\mu}) d\vec{\mu}, \quad (33)$$

i. e., the 6-fold integral reduces to a 3-fold integral with a smooth integrand.

Generally, the integrals in Eq. (32) are computable with straightforward Gaussian quadrature from Eq. (19), i. e.,

$$\begin{aligned} \overline{v_i v_i} \approx & 2 \sum_{k=1}^3 \sum_{k_1=0}^M \sum_{k_2=0}^M \sum_{k_3=0}^M w_{k_1} w_{k_2} w_{k_3} g_k((s_{k_1}, s_{k_2}, s_{k_3})) \times \\ & \times \sum_{\ell=1}^4 \sum_{k_4=0}^M \sum_{k_5=0}^M \sum_{k_6=0}^M w_{k_4} w_{k_5} w_{k_6} f_\ell^k((s_{k_1}, s_{k_2}, s_{k_3}), (s_{k_4}, s_{k_5}, s_{k_6})). \end{aligned}$$

3.1.2. Volumes with Positive Distance

Again, we transform the integral (17) to the reference volume V_{ref} using the transformations Λ_i and Λ_j from Section 2.1, i. e.,

$$\overline{v_i v_j} = \int_{V_i} \int_{V_j} k(\vec{x}_i, \vec{x}_j) d\vec{x}_i d\vec{x}_j = |V_i| |V_j| \int_{V_{\text{ref}}} \int_{V_{\text{ref}}} k(\Lambda_i(\vec{\alpha}), \Lambda_j(\vec{\beta})) d\vec{\beta} d\vec{\alpha}. \quad (34)$$

The integral kernel $k(\Lambda_i(\vec{\alpha}), \Lambda_j(\vec{\beta}))$ from Eq. (20) does not have singularities because $|\Lambda_i(\vec{\alpha}) - \Lambda_j(\vec{\beta})| > 0$ for all $\vec{\alpha}, \vec{\beta} \in V_{\text{ref}}$. Therefore, we may straightforwardly apply the

Gaussian quadrature from Eq. (19) to evaluate the integral, i.e.,

$$\overline{v_i v_j} \approx |V_i| |V_j| \sum_{k=0}^M \sum_{\ell=0}^M \sum_{m=0}^M \sum_{n=0}^M \sum_{p=0}^M \sum_{q=0}^M w_k w_\ell w_m w_n w_p w_q k(\Lambda_i((s_k, s_\ell, s_m)), \Lambda_j((s_n, s_p, s_q))).$$

3.2. Exponential decay of quadrature error

The following theorem can be proved along the lines of [21, Section 5.3.2.4]. It states that the quadrature error of the proposed numerical integration method decays exponentially with respect to the quadrature order M .

Theorem 3.1: *Let $\widetilde{v_i v_j}$ denote the approximation of the direct exchange area $\overline{v_i v_j}$ by Duffy transformation and Gaussian quadrature of order M as described in Section 3.1.1 for $V_i = V_j$ or by direct Gaussian quadrature of order M as described in Section 3.1.2 for $V_i \cap V_j = \emptyset$. Assume $\text{vis} = 1$. Then, there holds*

$$|\overline{v_i v_j} - \widetilde{v_i v_j}| \leq C |V_i| |V_j| \exp(-M),$$

where $C > 0$ depends only on d_k^i, d_k^j for $k = 1, 2, 3$. If the distance d between V_i and V_j is strictly positive, then C depends additionally on d . \square

As mentioned at the beginning of Sec. 3.2, the derivation of quadrature formulae for the cases where $V_i \neq V_j$ and $V_i \cap V_j$ is a common face, edge, or vertex, is similar to the given derivation for the case $V_i = V_j$. Moreover, the concept transfers also to volume-surface and surface-surface exchange areas. In particular, one can derive appropriate Duffy-type transformations such that the analogue of Theorem 3.1 also holds for these cases.

4. Example Problems

In this section, we present two example problems and a case study. The results demonstrate the accuracy, the low computational effort, and the applicability of the method to large-scale problems. In the first example problem, a non-convex geometry is analyzed and the results are validated based on satisfaction of the summation rules Eq. (15). In the second example, a benchmark problem is solved and the results are validated by comparison to values published in the literature. The case study demonstrates how the method can be utilized in a simulation model of an industrial strip annealing furnace. The results are validated by comparison with measurements from the real plant.

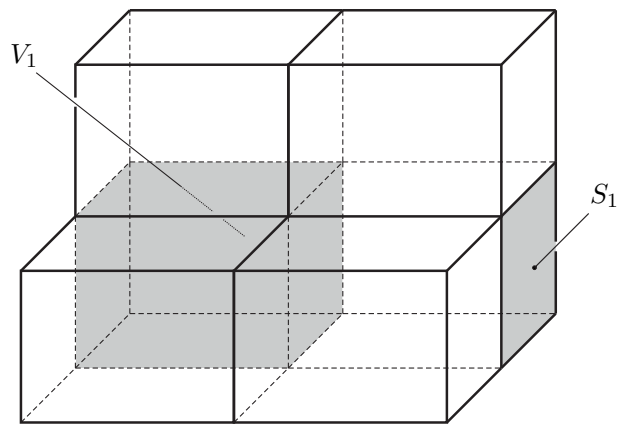


Figure 8. The enclosure of example problem 1 consists of $N_V = 6$ volume zones (left) and the corresponding $N_S = 22$ surface zones, which cover the boundary of the enclosure. For the comparison, we consider the highlighted zones V_1 and S_1 .

4.1. Example Problem 1

We consider the non-convex enclosure outlined in Fig. 8. Direct exchange areas are computed by the proposed method (coordinate transformations and Gaussian quadrature). For comparison, the problem is also solved by direct application of Gaussian quadrature (without coordinate transformations).

Because the exchange areas cannot be analytically computed, we check if the summation rules Eq. (15) are satisfied to validate the obtained results. Therefore, we first select a volume zone V_1 and a surface zone S_1 which are highlighted in Fig. 8. We define the relative error by measuring the relative violation of the summation rules, i.e., for the volume zone

$$\text{err}(V_1) := \left| \sum_{k=1}^{N_V} \widetilde{v_1 v_k} + \sum_{k=1}^{N_S} \widetilde{v_1 s_k} - 4K|V_1| \right| / (4K|V_1|)$$

and for the surface zone

$$\text{err}(S_1) := \left| \sum_{k=1}^{N_V} \widetilde{v_k s_1} + \sum_{k=1}^{N_S} \widetilde{s_1 s_k} - |S_1| \right| / |S_1|,$$

where $\widetilde{v_1 v_k}$, $\widetilde{v_1 s_k}$, $\widetilde{v_k s_1}$, and $\widetilde{s_1 s_k}$ are the approximations of the respective direct exchange areas. These approximations are obtained by using (first) the quadrature rules from Section 3 and (second) standard tensor Gaussian quadrature as for the case of non-touching zones in Section 3.1.2. We will denote the latter approach as the direct approach.

In the case of $\widetilde{v_1 v_k}$ and direct tensor Gaussian quadrature, we use M quadrature points per dimension for the outer three integrals and $M + 1$ quadrature points per dimension for the three inner integrals (otherwise the integrand is evaluated at the singularity). The

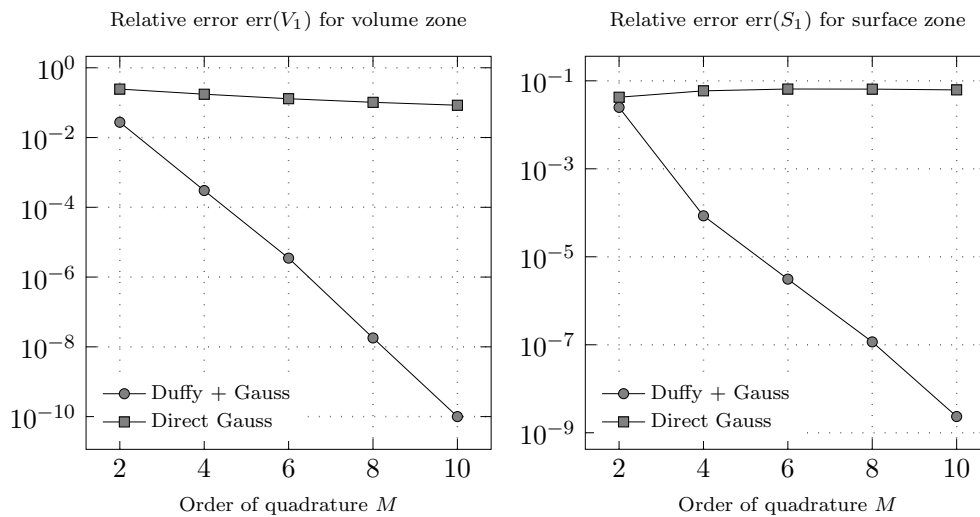


Figure 9. Comparison of example problem 1 in terms of the relative errors $\text{err}(V_1)$ and $\text{err}(S_1)$ of the summation property Eq. (15) using either the presented quadrature rules (Duffy + Gauss) or standard Gaussian quadrature rules (direct Gauss).

comparison is shown in Fig. 9.

We observe a significant improvement for the volume zone and for the surface zone. The direct quadrature does not even seem to converge for the surface zone. This underlines the necessity of using proper quadrature formulas to evaluate singular integrals.

4.2. Example Problem 2

For simple rectangular geometries consisting of cubes ($N_V = 2$ volume zones) and squares ($N_S = 10$ surface zones), exchange areas can be found in published tables and charts, see [1, 10, 12, 25]. In the following, a simple example of an industrial furnace presented in [10] is used as a benchmark. In this example, the exchange area $\overline{v_1 \overline{L}}$ between a participating gaseous medium in the rectangular furnace chamber represented by V_1 and V_2 and the load represented by the gray surface sections is determined (cf. Fig. 10). The accuracy of the result is checked based on values published in [10] and based on the summation rules Eq. (15).

As outlined in Fig. 10, the discretized geometry of the considered furnace chamber consists of two adjacent cubic gas volumes bounded by square surface zones with a side length of $B = 2$ m. This discretization is chosen based on the available exchange areas published in [10]. The gas is assumed to have a constant absorption coefficient $K = 0.16 \text{ m}^{-1}$. The load is shown as a gray shaded surface. Selected exchange areas required for determining the radiative heat transfer inside the enclosure are given in Tab. 1. The left column contains the exchange areas presented in [10]. The exchange area $\overline{v_1 \overline{v_1}}$ cannot be directly determined from [10] because of the associated singularities.

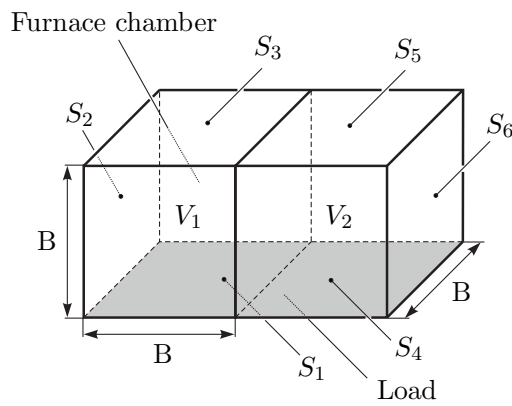


Figure 10. Discretized rectangular furnace chamber from example problem 2.

If required, this exchange area may be determined by using the summation rules Eq. (15). The right column contains the results obtained by using the proposed integration method with $M = 10$ quadrature points. The results agree very well with those from [10].

Table 1. Selected direct exchange areas for the enclosure from example problem 2 (cf. Fig. 10).

	[10]	Duffy + Gauss
$\overline{s_1 s_2}$	0.67742	0.67410
$\overline{s_1 s_3}$	0.56111	0.56063
$\overline{s_1 s_4}$	0.11911	0.11911
$\overline{s_1 s_5}$	0.22709	0.22581
$\overline{s_1 s_6}$	0.07967	0.07968
$\overline{s_2 s_6}$	0.14144	0.14136
$\overline{v_1 v_2}$	0.12084	0.12084
$\overline{v_1 v_1}$	-	0.66222
$\overline{v_1 s_1}$	0.74611	0.74296
$\overline{v_1 s_6}$	0.09975	0.10054
$\overline{v_2 s_1}$	0.13078	0.13040

Taking into account the symmetry of the considered geometry and using the reciprocity rules Eq. (14), the desired exchange area $\overline{v s_L}$ can be determined by $\overline{v s_L} = 2\overline{v_1 s_1} + 2\overline{v_2 s_1}$. Thus, we obtain $\overline{v s_L} = 1.7538 \text{ m}^2$ according to [12] and $\overline{v s_L} = 1.7467 \text{ m}^2$ from the

developed integration method. To verify both results, the summation rule

$$S_L = \overline{s_L s_L} + \overline{s_W s_L} + \overline{v s_L} \quad (35)$$

is checked. Here, S_L is the surface area of the load, $\overline{s_L s_L} = 0$ is the self-interaction of the load, and $\overline{s_W s_L} = 6\overline{s_1 s_2} + 2\overline{s_1 s_3} + 4\overline{s_1 s_4} + 2\overline{s_1 s_5} + 2\overline{s_1 s_6}$ is the exchange area between the remaining surfaces and the load. Using the results from [12], Eq. (35) yields $S_L = 8.03 \text{ m}^2$, which is close to the true value of the surface area 8 m^2 . With the proposed integration method, the surface area $S_L = 8 \text{ m}^2$ according to Eq. (35) matches exactly the real value, i.e., the summation rule is exactly fulfilled. This result demonstrates the high accuracy of the developed integration method that systematically takes into account the singularities.

We stress that the proposed method is not limited to cubes and squares, i.e. the desired exchange area $\overline{v s_L}$ can also be directly determined by applying the proposed method to the corresponding 5-fold integral (9). This example was presented for benchmark purposes. In the next section, a more challenging radiation enclosure with obstacles is analyzed. For this geometry, we cannot simply use tabulated exchange areas from the literature.

4.3. Case Study - Industrial Furnace

We consider a direct-fired continuous strip annealing furnace, where steel strips are heated by means of hot flue gas which stems from the combustion of natural gas [26, 27, 28]. The flue gas contains molecules like water and carbon dioxide, which have non-symmetrical oscillation patterns [3]. This is why the flue gas constitutes a participating medium and has to be considered in an analysis of the radiative heat exchange. Thermal radiation is the dominant heat transfer mechanism in this furnace due to the high temperatures [11]. For a simulation model of the considered furnace, the radiative heat transfer should be accurately captured. To avoid the effort of computing direct exchange areas for the zone method, various simplified approaches have been proposed in the literature on furnace modeling [27, 29, 30]. In [27], for example, furnaces are considered as tubes and are discretized in the longitudinal direction into finite volume zones. In each volume zone, the radiative heat transfer is modeled by a local radiation balance with simplified two-dimensional direct exchange areas [31], i.e., there is no radiative interaction in the longitudinal direction.

A simulation model of the furnace considered here has been presented in [28]. Based on this model, the capabilities of the proposed method for calculating direct exchange areas

are demonstrated. To that end, two versions of the model are considered: In version 1, the zone method is applied and the integration method proposed in this paper is used to calculate the direct exchange areas. That is, thermal radiation is considered as a three-dimensional problem in version 1 of the model. In version 2 of the model, radiative heat transfer is modeled as a two-dimensional problem as proposed in [27].

Fig. 11 shows the considered furnace of voestalpine Stahl GmbH, Linz, Austria, which is characterized by the parameters listed in Tab. 2. The counterflow furnace consists of

Table 2. Parameters of the furnace from the case study.

Parameter	Value
Strip velocity	90 – 180 m/min
Strip thickness	0.35 – 1.2 mm
Strip width	800 – 1700 mm
Length of furnace	50 m

a preheater, a post combustion chamber, and four heating zones A–D with gas burners. Due to the combustion of natural gas, energy is released and the strip is heated. The strip is conveyed through the furnace by three rolls. At the end of the furnace, the strip temperature is measured by a pyrometer. Additionally, thermocouples are installed in the heating zones to measure the local wall temperatures.

In Sec. 4.3.1, an overview of the simulation model is given. A simulation study is carried out based on both versions of the model. In Section 4.3.2, the model is verified by means of measurements from the real plant.

4.3.1. Overview of the Simulation Model

The proposed furnace model (cf. [28]) consists of submodels for the combustion, the flue gas, the rolls, the strip, and the walls. These submodels are interconnected by means of the heat transfer mechanisms conduction, convection, and radiation, see Fig. 12. The furnace has been discretized into volume zones, which are considered as well-stirred reactors. In the submodels, the mass, the enthalpy, and the heat balance as well as chemical reaction equations have been applied to capture the dynamic behavior and thermal radiation has been modeled by the zone method. The flue gas volume constitutes the volume zones. The rolls, the strip, and the walls constitute the surface zones. The submodels are assembled to a dynamical model, which can be written in the state-space

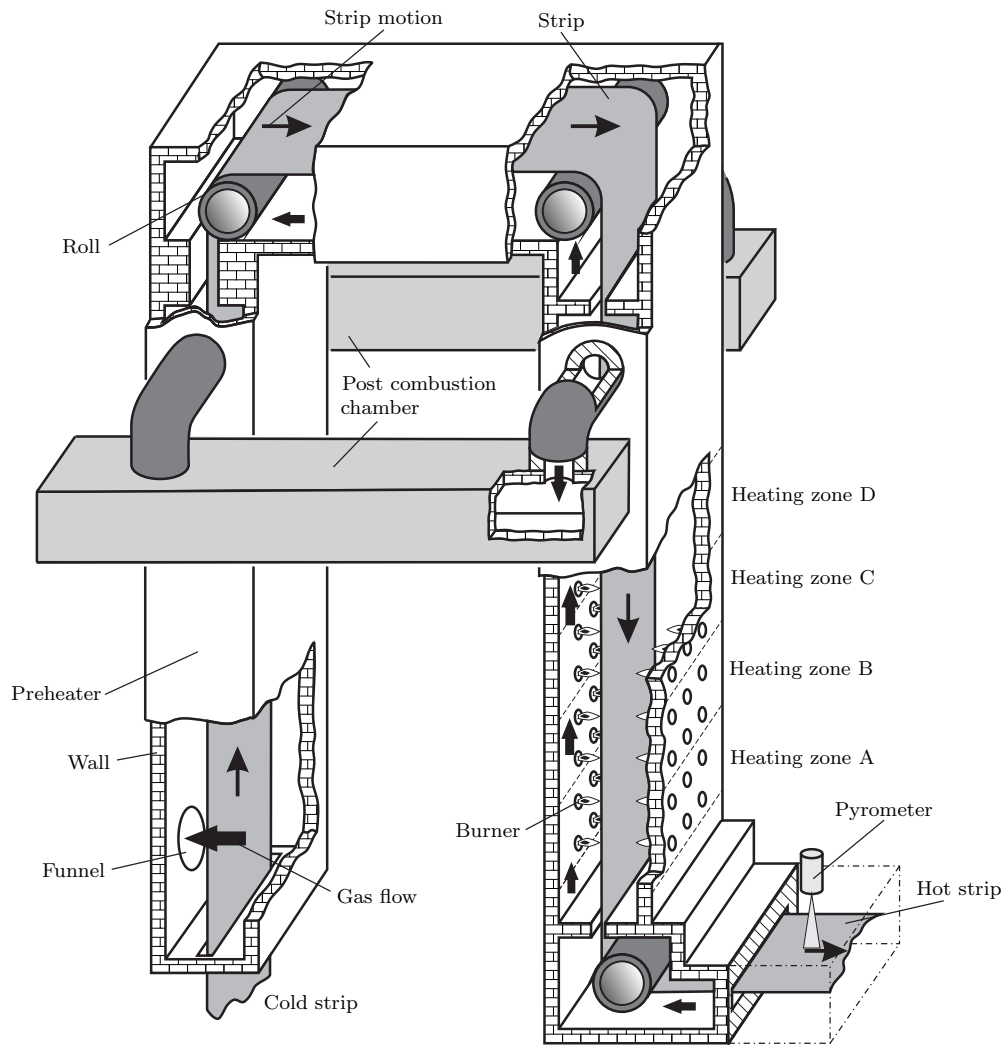


Figure 11. Schematic of the strip annealing furnace [28] analyzed in the case study.

form

$$\frac{d}{d\tau} \mathbf{x} = \mathbf{f}(\tau, \mathbf{x}, \mathbf{u}) \quad (36)$$

(cf. [28]) with the time τ and the state vector \mathbf{x} . Eq. (36) also captures the heat flows due to thermal radiation. Moreover, the system input \mathbf{u} includes the air and fuel supply to the burners, the strip velocity, the strip thickness and width, and the steel grade.

4.3.2. Verification of the Simulation Model

The simulation results have been computed by both versions of the considered mathematical model and are compared to data recorded at the real plant. Fig. 13 shows a comparison of the strip temperature at the end of the furnace, where the pyrometer is

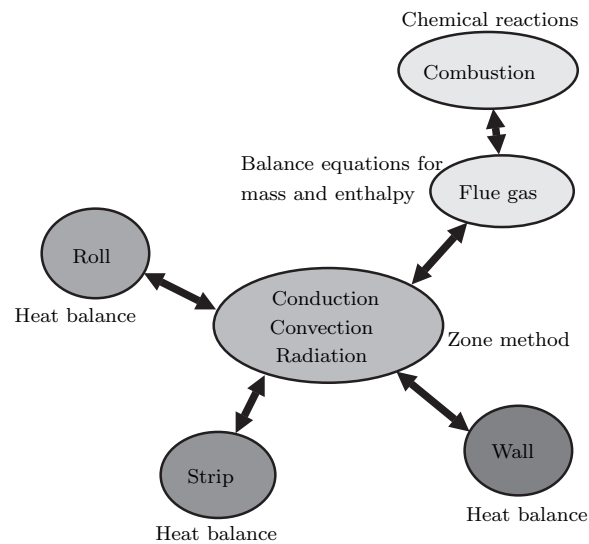


Figure 12. Submodels of the furnace considered in the case study.

located. This figure indicates the good accuracy achieved by the furnace model version 1,

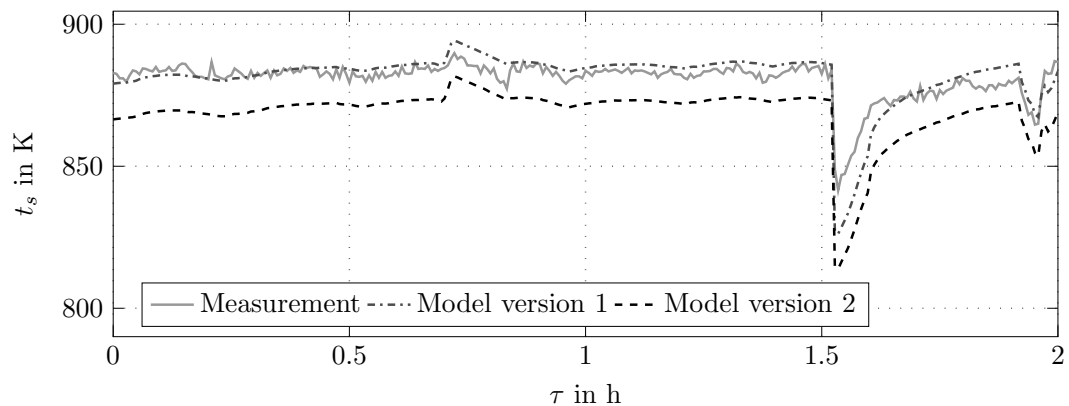


Figure 13. Strip temperature at the end of the furnace considered in the case study.

where both the steady-state and the transient operation are well captured. Version 2 is characterized by a similar dynamical behavior, however, an offset occurs. Fig. 14 shows a comparison of the simulated and the measured wall temperature t_w in the heating zone C. These results demonstrate the good accuracy achieved by both versions of the furnace model. However, version 1 performs better than version 2 due to the more detailed submodel of the radiative heat transfer. This case study demonstrated the benefit of the proposed integration method for an industrial scenario.

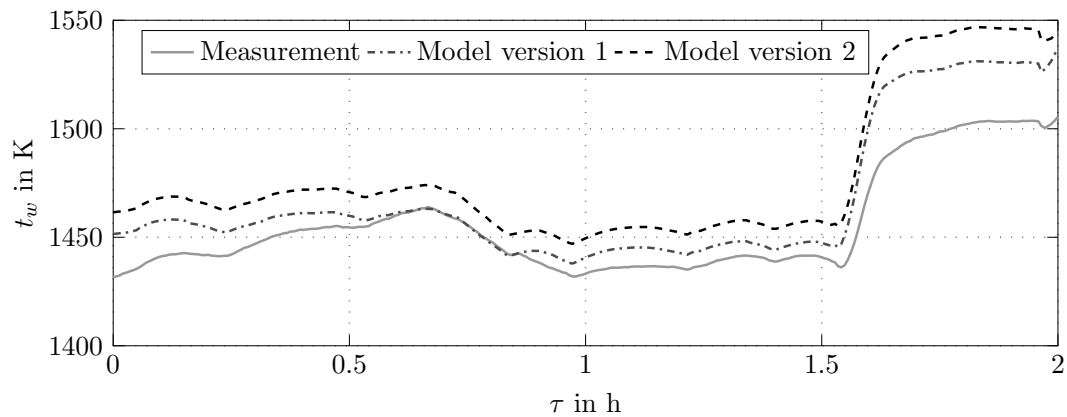


Figure 14. Wall temperature in the heating zone C of the furnace considered in the case study.

5. CONCLUSIONS

The original results and findings of this work are the following: We derived coordinate transformations for the calculation of direct exchange areas which distribute points with singularities to larger domains. This eliminates the singularities, leads to smooth kernels, and allows for a rigorous mathematical analysis of the quadrature error. The approach is an effective cure for the significant and so-far unsolved problem of singularities in the calculation of direct exchange areas. The proposed method can treat non-convex geometries which require the consideration of a visibility function as mentioned in Section 2.2. Here, the computational load can be reduced if geometry elements are hierarchically clustered. In case of constant visibility (i.e. $\text{vis} = 1$), the integral reduces to a lower dimensional integral. The developed method was validated based on numerical results, results published in the literature, and measurements from an industrial plant. The method is not restricted to the computation of direct exchange areas and may be utilized in a similar way for more general singular integral kernels.

ACKNOWLEDGMENT

This research was financially supported by the Austrian Research Promotion Agency (FFG), grant no.: 834305. Moreover, the authors are grateful to the industrial research partners voestalpine Stahl GmbH and Andritz AG. The research of the authors MF, TF, and DP is supported through the FWF project *Adaptive Boundary Element Method*, funded by the Austrian Science fund (FWF) under grant P21732, see <http://www.asc.tuwien.ac.at/abem>. The authors MF and DP acknowledge the support of the FWF doctoral program “*Dissipation and Dispersion in Nonlinear PDEs*” under grant W1245, see <http://npde.tuwien.ac.at/>. The author AS gratefully ac-

knowledges financial support provided by the Austrian Academy of Sciences in the form of an APART-fellowship at the Automation and Control Institute of Vienna University of Technology.

REFERENCES

1. H.C. Hottel and E.S. Cohen. Radiant heat exchange in a gas filled enclosure: Allowance for non-uniformity of gas temperature. *American Institute of Chemical Engineering Journal*, 4:3–14, 1958.
2. R. Siegel and J.R. Howell. *Thermal Radiation Heat Transfer*. Taylor & Francis, New York, London, 4th edition, 2002.
3. M.F. Modest. *Radiative Heat Transfer*. Academic Press, New York, 2nd edition, 2003.
4. H.C. Hottel and A.F. Sarofim. *Radiative Transfer*. McGraw-Hill, New York, 1967.
5. H.D. Baehr and K. Stephan. *Heat and Mass Transfer*. Springer, Berlin Heidelberg, 2nd edition, 2006.
6. A. Faghri, Y. Zhang, and J.R. Howell. *Advanced Heat and Mass Transfer*. Global Digital Press, Columbia, MO, 2010.
7. J.R. Howell. Thermal radiation in participating media: The past, the present, and some possible futures. *Transactions of the ASME, Journal of Heat Transfer*, 110(4b):1220–1229, 1988.
8. Y.S. Kocaeffe, A. Charette, and M. Munger. Comparison of the various methods for analysing the radiative heat transfer in furnaces. *Proceedings of the Combustion Institute Canadian Section Spring Technical Meeting, Vancouver, Canada*, pages 15–17, May 1987.
9. S.C. Mishra and M. Prasad. Radiative heat transfer in participating media – A review. *Sādhanā - Academy Proceedings in Engineering Sciences*, 23(2):213–232, 1998.
10. J.M. Rhine and R.J. Tucker. *Modelling of Gas-Fired Furnaces and Boilers and Other Industrial Heating Processes*. McGraw-Hill, London, UK, 1991.
11. R. Viskanta and M.P. Mengüç. Radiation heat transfer in combustion systems. *Progress in Energy and Combustion Science*, 13(2):97–160, 1987.
12. R.J. Tucker. Direct exchange areas for calculating radiation transfer in rectangular furnaces. *Transactions of the ASME, Journal of Heat Transfer*, 108(3):707–710, 1986.
13. H. Errku. *Radiant heat exchange in gas-filled slabs and cylinders*. PhD thesis, Massachusetts Institute of Technology, Cambridge, MA, 1959.
14. W. Tian and W.K.S. Chiu. Calculation of direct exchange areas for nonuniform zones using a reduced integration scheme. *Transactions of the ASME, Journal of Heat Transfer*, 125(5):839–844, 2003.
15. J. Sika. Evaluation of direct-exchange areas for a cylindrical enclosure. *Transactions of the ASME, Journal of Heat Transfer*, 113(4):1040–1044, 1991.
16. W. Tian and W.K.S. Chiu. Hybrid method to calculate direct exchange areas using the

- finite volume method and midpoint integration. *Transactions of the ASME, Journal of Heat Transfer*, 127(8):911–917, 2005.
17. J.C. Chai, J.P. Moder, and K.C. Karki. A procedure for view factor calculation using the finite-volume method. *Numerical Heat Transfer, Part B: Fundamentals*, 40(1):23–35, 2001.
 18. H. Ebrahimi, A. Zamaniyan, J.S.S. Mohammadzadeh, and A.A. Khalili. Zonal modeling of radiative heat transfer in industrial furnaces using simplified model for exchange area calculation. *Applied Mathematical Modelling*, 37(16-17):8004–8015, 2013.
 19. A. Kheiri, J.L. Tanguier, D. Bour, R. Mainard, and J. Kleinclaus. Transfert de chaleur dans les milieux semi-transparents: adaptation de la méthode des zones de Hottel aux milieux optiquement épais. *Proceeding of the SFT-90 Colloque de Thermique, Nantes, France*, 2:37–40, May 1990.
 20. J.M. Goyhénèche and J.F. Sacadura. The zone method: A new explicit matrix relation to calculate the total exchange areas in anisotropically scattering medium bounded by anisotropically reflecting walls. *Transactions of the ASME, Journal of Heat Transfer*, 124(4):696–703, 2002.
 21. S.A. Sauter and C. Schwab. *Boundary Element Methods*, volume 39 of *Springer Series in Computational Mathematics*. Springer-Verlag, Berlin, 2011.
 22. L. Greengard and V. Rokhlin. A fast algorithm for particle simulations. *Journal of Computational Physics*, 73(2):325–348, 1987.
 23. H. Cheng, L. Greengard, and V. Rokhlin. A fast adaptive multipole algorithm in three dimensions. *Journal of Computational Physics*, 155(2):468–498, 1999.
 24. S. Börm, L. Grasedyck, and W. Hackbusch. Introduction to hierarchical matrices with applications. *Engineering Analysis with Boundary Elements*, 27(5):405 – 422, 2003.
 25. H.B. Becker. A mathematical solution for gas-to-surface radiative exchange area for a rectangular parallelepiped enclosure containing a gray medium. *Journal of Heat Transfer*, 99:203–207, May 1977.
 26. K.S. Chapman, S. Ramadhyani, and R. Viskanta. Modeling and analysis of heat transfer in a direct-fired continuous reheating furnace. *Heat Transfer In Combustion Systems*, 122:35–44, 1989.
 27. D. Marlow. Modelling direct-fired annealing furnaces for transient operations. *Applied Mathematical Modelling*, 20(1):34–40, 1996.
 28. S. Strommer, M. Niederer, S. Steinboeck, and A. Kugi. A mathematical model of a direct-fired continuous strip annealing furnace. *International Journal for Heat and Mass Transfer*, 69:375–389, 2014.
 29. A. Jaklič, F. Vode, and T. Kolenko. Online simulation model of the slab-reheating process in a pusher-type furnace. *Applied Thermal Engineering*, 27:1105–1114, 2007.
 30. C.-K. Tan, J. Jenkins, J. Ward, J. Broughton, and A. Heeley. Zone modelling of the thermal performances of a large-scale bloom reheating furnace. *Applied Thermal Engineering*, 50:1111–1118, 2013.
 31. J.P. Holman. *Heat Transfer*, volume 10. McGraw Hill, 2010.